Available online at www.sciencedirect.com
SCIENCE DIRECT
Biochimie 88 (2006) 583–593
BIOCHIMIE
www.elsevier.com/locate/biochi

Plant metallothionein domains: functional insight into physiological metal binding and protein folding

Jordi Domènech [a], Gisela Mir [b], Gemma Huguet [b], Mercè Capdevila [c], Marisa Molinas [b], Sílvia Atrian [a,*]

[a] Departament de Genètica, Facultat de Biologia, Universitat de Barcelona, Av. Diagonal 645, 08028 Barcelona, Spain
[b] Departament de Biologia, Universitat de Girona, Campus Montilivi, 17071 Girona, Spain
[c] Departament de Química, Facultat de Ciències, Universitat Autònoma de Barcelona, 08193 Barcelona, Spain

Received 4 April 2005; accepted 4 November 2005
Available online 01 December 2005

Abstract

Plant metallothioneins (MTs) differ from animal MTs by a peculiar sequence organization consisting of two short cysteine-rich terminal domains linked by a long cysteine-devoid spacer. The role of the plant MT domains in the protein structure and functionality is largely unknown. Here, we investigate the separate domain contribution to the in vivo binding of Zn and Cu and to confer metal tolerance to *CUP1*-null yeast cells of a plant type 2 MT (QsMT). For this purpose, we obtained three recombinant peptides that, respectively, correspond to the single N-terminal (N25) and C-terminal (C18) cysteine-rich domains of QsMT, and a chimera in which the spacer is replaced with a four-glycine bridge (N25–C18). The metal–peptide preparations recovered from Zn- or Cu-enriched cultures were characterized by ESI-MS, ICP-OES and CD and UV–vis spectroscopy and data compared to full length QsMT. Results are consistent with QsMT giving rise to homometallic Zn- or Cu-MT complexes according to a *hairpin* model in which the two Cys-rich domains interact to form a cluster. In this model the spacer region does not contribute to the metal coordination. However, our data from Zn-QsMT (but not from Cu-QsMT) support a fold of the spacer involving some interaction with the metal core. On the other hand, results from functional complementation assays in endogenous MT-defective yeast cells suggest that the spacer region may play a role in Cu-QsMT stability or subcellular localization. As a whole, our results provide the first insight into the structure/function relationship of plant MTs using the analysis of the separate domain abilities to bind physiological metals.

Keywords: Metallothionein; *Quercus suber*; Separate Cys-rich domains; Spacer region; Zn-aggregates; Cu-aggregates; MT dimers; Yeast complementation

1. Introduction

Metallothioneins (MTs) are small cysteine-rich proteins with the ability to coordinate heavy metal atoms. Although widely distributed among the animal and plant kingdoms, MTs show an extremely heterogeneous composition. They are currently clustered in 15 families following taxonomical criteria [1]. Paradigmatic mammalian MTs contain two cysteine-rich domains (9 and 11 cysteine residues) that fold into two independent metal clusters joined by a two to three non-cysteinic amino acid hinge when coordinating divalent metal ions. Plant MTs, placed in Family 15, generally contain two smaller cysteine-rich domains (four to eight cysteine each) and a large spacer region (30–50 residues) devoid of this amino acid. The distribution of cysteine residues, as well as the length of the spacer region served to further classify plant MTs into four types [2,3], as shown in Table 1. Only a reduced number of plant MTs differ from these canonical primary structures: the type 4 MTs, characterized by three cysteine-rich regions, and the *Brassicaceae* subtype in type 1 MTs, bearing a short

Table 1
Classification of plant MT according to the cysteine motifs in their N- and C-terminal regions and the length of the corresponding spacer regions, adapted from [3]

Type 1	(2-4)xCxCxxxCxCxxxCxC…39 to 45…CxCxxxCxCxxCxC(0-2)x
subtype B	5xCxCxxxCxCxxxCxC …7… CxxCxCxxxCxCxxxCxC
Type 2	xxCCxxxCxCxxxCxCxxxCxxC…37 to 49…CxCxxxCxCxxCxC(0-2)x
Type 3	(2-4) xCxxCxCxxxxxC…32 to 34…CxCxxxCxCxxCxC(0-2)x
Type 4	2xCxxxCxCxxxCxxxxxCxC…12,14…CxCxxxCxCxxCxC…15…CxCxxxCxCxxC5x

* Corresponding author. Tel.: +34 93 402 1501; fax: +34 93 403 4420.
E-mail address: satrian@ub.edu (S. Atrian).

0300-9084/$ - see front matter © 2005 Elsevier SAS. All rights reserved.
doi:10.1016/j.biochi.2005.11.002

(less than 10 residues) spacer. In *Arabidopsis* seven actively expressed MT genes have been identified that include representatives of the four types [3,4]. The further isolation of representatives for the four types in the distant model *Oryza sativa* (rice) indicated that the multiplicity of MT forms precedes the dicot/monocot split in Angiosperms, and suggests that it is a common feature among all this group of plants. Single MT forms have been also isolated in Gymnosperms [5] and algae (*Fucus vesiculatus*) [6].

In contrast to the huge amount of knowledge about animal MTs, including NMR data [7], the structural and functional properties of plant MTs are still largely unknown (for plant MTs review see [2,3]). In general, plant MTs respond to a great variety of stresses (metal ions, abscisic acid, salt and oxidative stress, bounds and pathogen invasions) with a ubiquitous expression [8]. Some trends of spatial distribution points to an increased type 2 expression in aerial organs, while type 1 preferential synthesis seems located in the subterranean tissues [3,9]. Type 3 MT mRNAs have been mainly purified from ripening fruits [10] and type 4 is especially abundant in seeds [11]. Several attempts have also been devoted to determine the specificity of the metal response of plant MTs, and it is generally accepted that plant MTs play a role related to copper homeostasis or metabolism, on the basis of the reported induction of several MT genes by copper [12,13]. Moreover, a correlation between MT gene expression and copper tolerance has been observed in *Arabidopsis* and *Silene* ecotypes [14,15] and the ability of some plant MT proteins to functionally bind copper in both yeast and *E. coli* cells [16–18] has been demonstrated. On the other hand, Zn and Cd also induce some plant MT gene response [13,18] yielding the corresponding metal-MT aggregates [16,10,18]. Recently, it has been shown that expression of *Arabidopsis* MT2a and MT3 in *Vicia* guard cells protect these cells from degradation upon exposure to Cd [19], this confirming that at least some plant MT may play a role in Cd detoxification in plants, concomitantly with Phytochelatins.

However, advances in plant MT knowledge have been impaired by the high level of proteolysis associated to native protein purification. Unfortunately, many efforts of recombinant (*E. coli*) plant MT synthesis did not enable to overcome this drawback [20], and consequently, the characterization of the putative metal-aggregates formed by plant MT remained unsolved. Recently, and using a GST-based expression system in *E. coli* we obtained highly homogeneous preparations of undigested Cu, Zn and Cd aggregates from a plant MT (QsMT). QsMT is a type 2 plant MT isolated in our laboratory from a *Quercus suber* phellem cDNA library [21]. In situ hybridization results showed then that this gene was actively induced in response to oxidative stress, either endogenous (suberization and proliferating tissues) or exogenous (paraquat or H_2O_2). However, parallel experiments to test the increase of QsMT synthesis in response to elevated Zn or Cu failed to reveal significant differences with the control samples. We had previously used the GST-system for the study of some animal MTs (*Drosophila* [22,23], *Crustacea* [24], mammalian MT1 [25] and MT4 [26]) and the protein domain contribution to metal coordination could be ascertained by means of high resolution spectroscopic and spectrometric analyses [24,27,28]. Applying the same rationale, we characterized the basic features of QsMT metal clusters, which were consistent with a copper related biological role, maybe related with its redox potentiality [29], confirmed by the capacity of QsMT to complement copper tolerance in a MT-null yeast mutant [21]. Albeit the characterization of the entire QsMT metal aggregates, the particular contribution of the different plant MT domains to the protein structure and function remained unclear. Here, we aim at shedding light on the role of plant MT domains in in vivo metal binding, by means of a protein dissection strategy. Two independent peptides consisting of the N-terminal (N25) and the C-terminal (C18) Cys-rich domains of QsMT, and a chimera (N25–C18) in which the spacer region is replaced with a short glycine bridge, were recombinantly synthesized as GST-fusion peptides. Then, the corresponding metal aggregates obtained from Zn and Cu enriched *E. coli* cultures were purified and characterized in comparison with those from the full length QsMT [21]. In addition, to further investigate the in vivo metal binding abilities of the full length QsMT, the Zn_4-QsMT species were titrated with Cu(I). Finally, the capacity of QsMT and of its three derived peptides to confer metal (Zn or Cu) tolerance to a yeast strain defective in its endogenous CUP1 MT was investigated. Overall, the results led us to propose a binding model for Zn- and Cu-QsMT species and to suggest a role for the MT spacer, a region that is highly conserved among plants but totally absent in animal MT.

2. Material and methods

2.1. Construction of the expression vectors

The cDNA sequences encoding for the independent N25 and C18 Cys-rich domains and the N25–C18 chimera (Table 2) were constructed using PCR-based strategies with the full length QsMT cDNA as a template [21] and Immolase (Bioline) as thermo resistant DNA polymerase. Enzyme activation (7 min at 95 °C) was followed by 30 cycles of PCR as follows: denaturation 45 s at 95 °C, hybridization 30 s at 55–60 °C, and elongation 45 s at 72 °C. For N25 (Met1-to-Met25), the upstream primer was N25/Bam (5′-CTCTGGATCCATGTCTTGCTGCGGA), which contains a *Bam*HI restriction site (underlined), the downstream primer was N25/Eco(5′ CGGAATTCTCACATCTTGCATCCTCCA) with an *Eco*RI restriction site (underlined) and a stop codon. For C18 (Asn61-to-Lys76), the upstream primer was C18/Bam (5′ CGGGATCCATGAATGGCTGCAAGTGC), which contains a *Bam*HI restriction site (underlined) and a start codon at the origin of the coding region, and the downstream primer was C18/Eco (5′-CGGAATTCTCATTTACAATTGCAAGGGTC) with *Eco*RI restriction site (underlined). For N25–C18, the N25 and C18 fragments were amplified separately and linked by a four-glycine encoding bridge using a two-step PCR. In this case the downstream primer for N25 was N25/Gly (5′-TCCTCCTCCTCCCATCTTGCATCCTCCACA), which contains the coding sequence for the four Gly bridge (underlined), and for C18 the upstream primer was C18/Gly (5′-GGAGGAG

Table 2
Amino acid sequences of the wild type QsMT form and the three deletion mutants. N25 corresponds to the QsMT N-terminal region containing the first eight Cys; C18 corresponds to the QsMT C-terminal region containing the last six Cys; and N25–C18 is the fusion of the N25 and C18 regions through a bridge of four Gly (solid box), so that this peptide lacks the spacer region of QsMT. Additional Gly and Ser (dotted box) are added to the N-terminal of the four peptides, due to the recombinant expression strategy

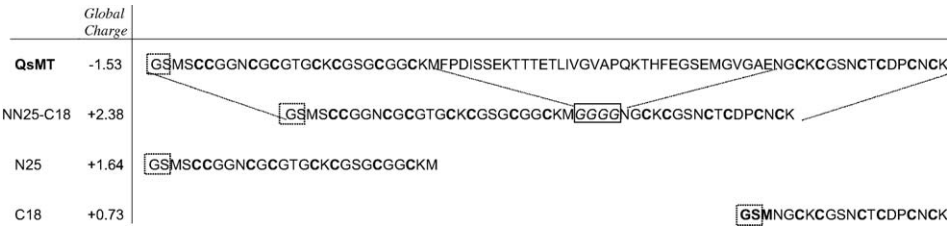

GAGGAAATGGCTGCAAGTGCGGCTG), which contains the complementary sequence for the Gly bridge (underlined). In order to optimize the hybridization and sequence filling reaction, equal amounts of N25 and C18 cDNA were subjected to 15 PCR cycles (denaturation 1 min at 94 °C, hybridization 30 s at 41 °C, elongation 45 s at 72 °C). The PCR products were diluted 1/25 and subjected to further PCR (30 cycles) using N25/Bam and C18/Eco primers (denaturation 45 s at 94 °C, hybridization: 30 s at 60 °C, elongation 45 s at 72 °C). The final PCR product was analyzed by agarose gel electrophoresis and ethidium bromide staining and the bands showing the expected size were excised and sequenced in an Applied Biosystems ABIPRISM 310 Automatic Sequencer using ABIPRISM Dye Terminator-Cycle Sequencing Ready reaction kit (Perkin Elmer).

The N25, C18 and N25–C18 cDNAs were subcloned in pGEX-4T2 (Amersham Pharmacia Biotech) to synthesize the encoded peptides fused to the C-terminal end of glutathione-S-transferase (GST) in *E. coli*, using the same procedure described in [21]. BL21 cells were transformed with the ligation mixtures, the corresponding plasmids recovered and the integrity of their coding regions was confirmed by DNA sequencing.

2.2. Purification and characterization of the recombinant metallopeptides

The recombinant peptides were biosynthesized in 3 l Luria Bertini (LB) medium, inoculated with 300 ml of overnight precultures of transformed *E. coli* cells. Induction with isopropyl β-D-thiogalactopyranoside (IPTG) was performed at OD_{600} = 0.8, and cultures were further grown for 3 h in the presence of 500 μM $CuSO_4$ or 300 μM $ZnCl_2$. Cells were harvested by centrifugation (Sorvall RC5C, 15 min at 9600 × *g*), resuspended in PBS, and lysed by sonication (Branson Sonifier 250, 0.6 Hz) in the presence of 0.5% β-mercaptoethanol to avoid protein oxidation. From this step on, all procedures were carried out using Ar (pure grade 5.6) saturated buffers. After sonication, the cellular debris was pelleted (20 min at 20000 × *g*) and GST–MT fusions were isolated from the supernatant by glutathione-sepharose 4B (Amersham Pharmacia) affinity chromatography. Metal–peptide aggregates were readily separated from GST by thrombin cleavage, so that the use of glutathione was avoided, and several concentration rounds were performed by Centriprep Microcon 3 (Amicon). Finally the metallopeptides were purified through FPLC in a Superdex75 column (Amersham Pharmacia Biotech) equilibrated with 50 mM Tris–HCl, pH 7.0. Selected fractions were confirmed by 15% SDS-PAGE and kept at –70 °C until further use.

The S, Zn and Cu content of the recombinant metallopeptide preparations was analyzed by inductively coupled plasma optic emission spectroscopy (ICP-OES). A Polyscan 61E (Thermo Jarrell Ash) spectropolarimeter was used, measuring Cu at 324.803 nm, S at 182.040 nm and Zn at 213.856 nm. Samples, acidified to a 1 M HCl final concentration, were analyzed as described in [30]. Protein concentration was calculated from the S value assuming that all S atoms in the sample were contributed by the metallopeptide: N25, 10 S atoms per molecule (eight Cys plus two Met); C18, seven S atoms per molecule (six Cys plus one Met); N25–C18, 16 S atoms per molecule (14 Cys plus two Met); and QsMT, 17 S atoms per molecule (14 Cys plus three Met). Protein concentration was confirmed by standard amino acid analysis performed on an Alpha Plus Amino acid Autoanalizer (Pharmacia LKB Biotechnology) after sample hydrolysis in 6 M HCl (22 h at 110 °C). The Ser, Lys and Gly content were used to extrapolate peptide concentrations.

2.3. Spectroscopic and spectrometric analyses of the Zn- and Cu-peptide complexes

UV–visible electronic absorption and CD analysis was carried out and processed as described in [31]. Electronic absorption measurements were performed on a HP-8453 diode array UV–visible spectrophotometer. A Jasco spectropolarimeter (J715) interfaced to a computer (J700 software) was used for CD determinations. The pH remained constant during the titration without the addition of buffers, and the temperature was kept at 25 °C by means of a Peltier PTC-351S apparatus. All spectra were recorded with 1 cm capped quartz cuvettes and processed using the GRAMS 32 program.

The molecular mass of the metal–peptide species was determined by electrospray ionization mass spectrometry (ESI-MS) performed on a Fisons Platform II Instrument (VG Biotech) controlled by the MassLynx Software and calibrated with horse heart myoglobin (0.1 mg/ml). Twenty microliters of the sample

were injected through a PEEK column (1 m × 0.007 in. i.d.) at 20 μl/min in the following conditions. For the in vivo samples: source temperature, 120 °C; capillary-counterelectrode voltage, 3.5 kV; lens-counterelectrode voltage, 1.5 kV; cone potential, 60 V. A *m*/*z* range from 750 to 1950 was scanned at 2 s/scan with an interscan delay of 0.2 s. The liquid carrier was acetonitrile/5 mM ammonium acetate pH 7 (20:80, v/v). The molecular mass of the in vitro samples was determined in the same way as the in vivo samples, except that source temperature was 90 °C; capillary-counterelectrode voltage, 3.0 kV and cone potential, 35 V. For apoform analysis, the metallopeptides were demetalated by acidification with HCl at pH 1.5, and mass spectrometry measures were carried out as explained for the holoforms except that the liquid carrier was methanol ammonium/formate ammonia, pH 2.5 (5:95, v/v). The molecular masses were calculated according to the method reported in [32].

2.4. Yeast functional complementation

For the yeast complementation assays two *Saccharomyces cerevisiae* strains were used: DTY3 (*MATα*, *leu2-3*, *112his3*$^{\Delta}$*1*, *trp1-1*, *ura3-50*, *gal1 CUP1*^{S}), that harbors only one copy of the endogenous *CUP1* gene, and DTY4 (DTY3 with *cup1::URA3*), totally deficient for *CUP1* [33], and hereafter referred in this paper to as *cup1*^{S} and *cup1*$^{\Delta}$, respectively. The cDNAs coding for N25, C18 and N25–C18 were excised from the corresponding pGEX recombinant plasmids (described above) by digestion with *Bam*HI/*Pst*I and ligated into the same sites of the yeast vector p424. The p424 vector contains TRP1 as a selection marker, and the recombinant sequences remain under the transcriptional control of the yeast constitutive glyceraldehyde-3-phosphate dehydrogenase (GPD) promoter and the cytochrome-c-oxidase (CYC1) terminator [34]. The p424 constructions were introduced into *cup1*$^{\Delta}$ cells using the lithium acetate procedure [35] and the transformed cells selected according to their capacity to grow in synthetic complete medium (SC) without Trp (p424 vector selection marker) and Ura (*cup1*$^{\Delta}$ strain selection marker) (SC-Trp-Ura medium).

For the metal tolerance tests, transformed *cup1*$^{\Delta}$ cells were initially grown in selective SC-Trp-Ura medium and *cup1*^{S} strain in SC medium, both at 30 °C and 220 rpm to OD_{600} = 0.5. Cultures were serially 10-fold diluted and 3 μl of each final sample spotted on SC plates with or without previously added $CuSO_4$ (75 μM for plate) or $ZnSO_4$ (7 mM for plate). Plates were incubated for 3 days at 30 °C and photographed.

3. Results and discussion

The QsMT-derived cDNA constructions coding for the two independent Cys-rich domains (N25 and C18) and for the N25–C18 chimera (Table 2) were confirmed by DNA sequencing and thereafter expressed in *E. coli* cells. The corresponding metal aggregates biosynthesized in Zn- or Cu-enriched media were analyzed by spectroscopic and spectrophotometric methods and data compared with those of the full length QsMT [21]. For each peptide, acidification at pH 1.5 of the recombinant metal-containing samples yielded single apoforms whose molecular masses were in accordance with the expected values calculated from their amino acid sequences (Table 3A). This confirmed the identity and the absence of endoproteolytic degradation for all recombinant peptides.

3.1. Zn-binding abilities and Zn-QsMT folding model

According to ICP-OES and ESI-MS data, N25–C18 synthesized in Zn-enriched medium yielded major Zn_4-peptide species, similarly to the full length QsMT. In contrast, N25 and C18 rendered mixtures of species with lower Zn/peptide ratios that, interestingly, included dimeric forms (Table 3B). Metal-MT species are identified by their ESI-MS peaks, which depend on the charge state-values within the scanned *m*/*z* range (*m*/*z*, *m* = molecular mass and *z* = charge). To assess the presence of MT dimers in the Zn–N25 and Zn–C18 preparations we applied a deconvolution method [36] that allowed us to identify two types of ESI-MS peaks that corresponded, respectively, to the dimeric forms: i) peaks that matched the *m*/*z* charge states of a $(Zn_n–MT)_2$ form (being *z* = odd value), and ii) peaks that only matched the molecular weight of two peptide chains binding an odd number of Zn(II) ions. Furthermore, some peaks could be either interpreted as corresponding to a monomer of *m*/*z* or to a dimer of a 2*m*/2*z* ratio. Considering that dimers were not detected in apoN25 and apoC18 preparations, dimerization is not attributed to intermolecular peptide bonds, but rather to the metal aggregate constitution itself.

The comparison of the CD spectra revealed that N25, C18, N25–C18 and QsMT all share a low chirality profile (Fig. 1). However, only Zn_4-QsMT showed the expected exciton coupling typical of the Zn-MT complexes (centered at 240 nm) [25]. For Zn–N25 and Zn–C18, the spectra revealed the presence of non-proteic ligands, albeit of a different nature in each case. The Zn–N25 CD spectrum, although closely related to that of QsMT (with a maximum at 248 nm) shows a clear increase in absorption at higher wavelengths. This, together with an extra ligand of 32 Da, detected by ESI-MS, confirmed that sulfide (S^{2-}) participates in the Zn–N25 aggregates, in a similar way to that described for Cd-QsMT [21] and animal MTs [37]. Conversely, the Zn–C18 CD-fingerprint merely displayed an absorption centered at ca. 230 nm. This absorption could be assigned to chloride anions that cannot be ESI-MS detected [23,38]. The Zn_4–N25–C18 complex exhibited a peculiar CD-fingerprint, different from that of QsMT (Fig. 1), that could be reproduced by the combined features of the Zn–N25 and Zn–C18 CD spectra, indicating that the N25–C18 chimera would contain both chloride and sulfide extra ligands.

Two main alternatives have been proposed for the plant metal-MT structure: a *hairpin* model in which the two Cys-rich domains form a single metal cluster and the spacer remains as a non-ordered connecting loop [20]; and a two-domain *dumbbell* model, proposed for a kiwi type 3 MT [39], similar to the well-known structure of mammalian metal-MT aggregates when coordinating divalent metals [40]. A third theoreti-

Table 3
Protein concentrations and metal (Zn or Cu) to protein ratios of the recombinant metal-QsMT forms. A) Metal-to-peptide ratio results obtained for the metallopeptides purified from Zn- or Cu-supplemented media. B) ESI-MS results of the apoforms of the four recombinant peptides, obtained by acidification of the corresponding. Zn-aggregates

A

ESI-MS	QsMT	N25-C18	N25	C18
Expected MW	7816.8	4365.4	2406.8	2025.0
Observed MW	7816.4±0.7	4365.6±0.3	2406.2±0.6	2024.0±1.1

B

Metal supplemented	Peptide	ICP-OES [a]	Amino acid analysis [b]	ESI-MS [c]		
		Protein concentration (M) Metal-QsMT molar ratio		Major species Minor species	Expected MW	Measured MW
Zn	QsMT	*1.50 x 10⁻⁴* 4.2 Zn	*1.50 x 10⁻⁴*	**Zn_4-QsMT**	8070.4	8070.0±0.6
	N25-C18	*1.32 x 10⁻⁴* 3.6 Zn	*1.30 x 10⁻⁴*	**Zn_4-N25-C18**	4619.0	4620.0±0.6
	N25	*3.20 x 10⁻⁴* 2.2 Zn	*3.20 x 10⁻⁴*	Zn_3-N25	2596.0	2595.2±1.6
				Zn_7X-$(N25)_2$	5288.8	5289.6±1.2
				Zn_2-N25	2531.8	2532.4±0.9
				Zn_9-$(N25)_2$	2694.3	2693.9±0.7
	C18	*3.36 x 10⁻⁴* 1.8 Zn	*3.30 x 10⁻⁴*	**Zn_2-C18**	2150.3	2150.0±0.7
				Zn_1-C18	2087.1	2086.4±0.8
				Zn_5-$(C18)_2$	4364.3	4367.8±1.9
Cu	QsMT	*0.26 x 10⁻⁴* 1.5 Zn 4.7 Cu	*0.24 x 10⁻⁴*	**M_8-QsMT**	8324.0±3.6	8326.2±1.6
				M_9-QsMT	8383.5±2.9	8386.8±2.3
				M_7-QsMT	8257.6±2.9	8255.3±1.1
				M_4-QsMT	8070.4±1.7	8067.2±1.3
	N25-C18	*0.95 x 10⁻⁴* 2.1 Zn 4.0 Cu	*0.95 x 10⁻⁴*	**M_8-N25-C18**	4872.6±3.3	4870.3±0.8
				M_9-N25-C18	4935.6±3.3	4934.1±3.3
				M_7-N25-C18	4806.2±2.9	4808.1±1.8
				M_4-N25-C18	4619.0±1.7	4617.7±1.2
	N25	*0.32 x 10⁻⁴* 3.3 Cu	*0.33 x 10⁻⁴*	**Cu_4-N25**	2660.3	2658.1±0.9
				Cu_5-N25	2723.7	2720.2±1.5
	C18	*2.00 x 10⁻⁴* 4.3 Cu	*2.20 x 10⁻⁴*	**Cu_8-$(C18)_2$** [d]	4547.8	4548.8±1.3
				Cu_5-$(C18)_2$	4610.3	4612.5±1.1

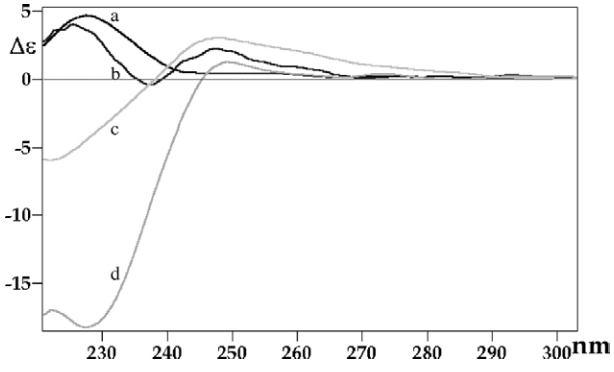

Fig. 1. CD spectra of the QsMT peptides synthesized in zinc-supplemented media. Comparison of the CD spectra corresponding to the Zn–C18 (a), Zn_4–N25–C18 (b), Zn–N25 (c) and Zn_4-QsMT (d) recombinant preparations.

cal *double dumbbell* model depending on MT dimerization is also conceivable (Scheme 1). Interestingly, structures with a hairpin model have been lately proposed for some unusual animal MTs [41]. According to our results, and on the basis of the differential arrangement of their metal clusters revealed by the CD data, different folding models should be assumed for Zn_4–N25–C18 and Zn_4-QsMT. Considering that the two Cys-rich domains act in an independent manner in Zn_4–N25–C18,

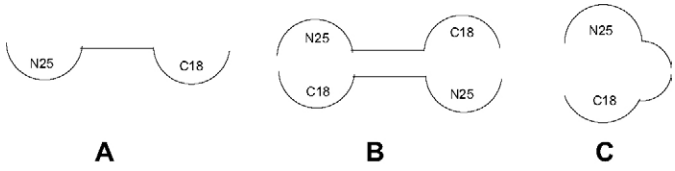

Scheme 1. Diagram showing the three putative models for the full-length QsMT folding.
A, Dumbbell; B, double dumbbell; and C, hairpin model.

the *dumbbell* model is the most plausible alternative in this case. Contrarily, the domain dependency described for Zn_4-QsMT leads to discard this model for QsMT. Then, between the *double dumbbell* and the *hairpin* model, both involving a N25/C18 interaction, we favor the second considering that dimeric Zn-QsMT species were never detected. Therefore, the *hairpin* model proposed for pea MT [20] remains as the most rational prospect for QsMT folding in the presence of Zn(II) ions. The differences between QsMT and N25–C18 CD spectra indicate that the spacer region, which encompasses eight charged residues and several potentially coordinating amino acids such as His, Asp or Glu, also contributes to the particular metal-cluster architecture. However, and somewhat paradoxically, the role of the spacer is not to facilitate the independency

of the two Cys-rich domains, but rather to make them mutually dependent when binding Zn. Any direct contribution of the spacer to Zn-coordination is discarded because N25–C18 and QsMT yield aggregates with an equivalent number of Zn ions, and because any of the well-known spectroscopic features associated with Zn–O or Zn–N chromophores was shown in the CD spectra. In summary, the spacer may play a stabilization role in Zn-aggregates. This region, through its side-chain negative charges, may adopt some fold interacting with the central metallic core that would account for the spectroscopical differences, without alteration of the binding capacity of the Cys-domains.

3.2. Cu-binding abilities and Cu-QsMT folding model

As for QsMT, N25–C18 yielded samples that contained both Zn(II) and Cu(I), in Cu-enriched medium, with major M_8-, and minor M_9-, M_7-, and M_4-species (Table 3B). In contrast, N25 and C18 rendered only homometallic Cu-aggregates when independently expressed. For N25, the major species was Cu_4–N25, with a minor presence of Cu_5–N25. For C18, the major species were Cu_8–$(C18)_2$ and Cu_9–$(C18)_2$, suggesting that the separate C18 domain mainly achieves Cu-binding after dimerization. Comparison of the four CD spectra (Fig. 2) revealed high intensity fingerprints, except for Cu–N25 that stands out for its lower chirality. Although all CD spectra appear very similar, a closer examination reveals at least two interesting details that must be highlighted. On the one hand, the absorptions at ca. 245 nm, which are due to the presence in the sample of Zn-species, as explained below, are found in Cu–N25–C18 and Cu-QsMT, but are absent in N25 and C18. On the other hand, all peptides show a common behavior in 280–380 nm region (Fig. 2, inset A1), with only Cu–N25 differing slightly in the low intensity peaks at 335–380 nm (Fig. 2, inset A2).

Taking into consideration the above results, the *hairpin* model should also be proposed for the folding of Cu-QsMT. However, in this case we cannot envisage any structural significance for the spacer region, considering that Cu–N25–C18 and Cu-QsMT show the same behavior. The *dumbbell* model was disregarded because C18, the shorter and fewer-Cys containing peptide, needs to interact with another Cys-rich region to achieve Cu(I) binding. The *double dumbbell* model implies dimerization and this scenario has been found neither in Cu–N25–C18 nor in Cu-QsMT. In the case of Cu–N25, the unique complex whose structure does not imply interaction between two Cys-rich regions, the metal-aggregate exhibits a less intense CD fingerprint, suggestive of a poorer folding degree. Interestingly, Cu–N25 shows peculiar CD features in 330–390 nm range, a UV–vis absorbance region characteristic of intrametallic Cu–Cu bands [42], which some authors [43] have associated with digonal Cu(I) coordination environments. So that, N25 could provide a somewhat different coordination binding site for Cu(I) in respect to C18, N25–C18 and QsMT.

In an attempt to further investigate Cu(I) coordination to QsMT, we titrated the Zn_4-QsMT complex with

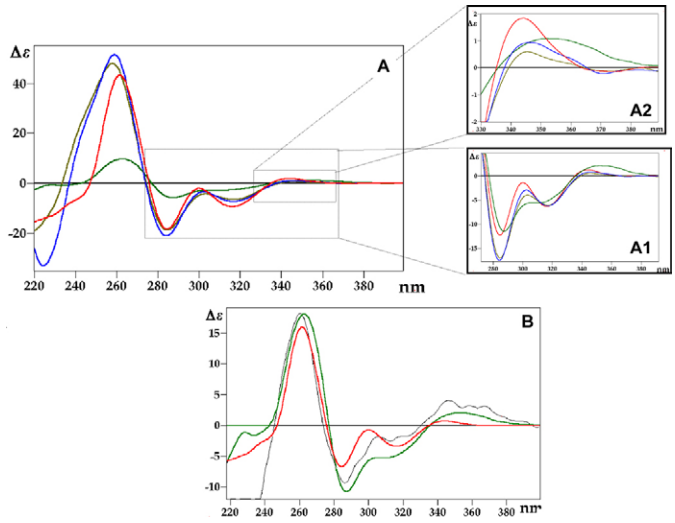

Fig. 2. CD spectra of the QsMT peptides synthesized in copper-supplemented media. (A) Comparison of the circular dichroism spectra corresponding to the Zn,Cu-QsMT (blue), Zn,Cu–N25–C18 (khaki), Cu–N25 (green) and Cu–C18 (red) recombinant preparations. (A1) and (A2) insets show normalized spectra for specific UV–vis regions. (B) Normalized circular dichroism spectra of Cu–N25 and Cu–C18, compared to that of the mammalian Cu_{10}-MT4 species (black solid line) (from Ref. [26]).

$(Cu(CH_3CN)_4)ClO_4$ at pH 7 and spectroscopically analyzed the progression of the Zn/Cu in vitro displacement reaction (full set of optical data in Fig. 3A–C). The Zn by Cu substitution proceeded isodichroically until the fourth Cu(I) eq was added. Although isodichroic evolutions are usually associated to cooperative processes, the ESI-MS and UV–vis difference data at this stage of the titration (M_4-, M_7-, M_8-, and M_9-major species) showed that this was not the case. Therefore, the direct conversion of Zn_4- to a putative Cu_4-QsMT species has to be discarded and thus M_4-QsMT would rather correspond to original Zn_4-QsMT aggregates that have not yet reacted with Cu (I). The CD fingerprint corresponding to the addition of the fifth Cu(I) eq to Zn_4-QsMT nicely matched that of the preparation of QsMT in Cu-supplemented medium (Fig. 4A), including the characteristic absorption at ca. 240 nm of the Zn-thiolate chromophores and attributable to remaining Zn_4-QsMT, this suggesting a comparable composition of both the in vivo and in vitro samples (Table 3B). When further aliquots of Cu(I) were added (up to 7 eq), the ESI-MS data showed coexistence of homometallic Cu_8- and Cu_9-QsMT complexes, with concomitant loss of the ca. 240 nm absorption. At this point, the CD fingerprint evolved to match that characteristic of homometallic Cu-QsMT species, which show an absorption centered at 350 nm comparable to that of the biosynthesized Cu–N25 species (Fig. 4B).

Unfortunately, and due to the closeness of Zn and Cu atomic weights [12,28], ESI-MS cannot inform if the mixed Zn,Cu composition of a sample is due to the presence of heterometallic M_x-QsMT complexes (M = Zn and Cu) or is the result of the coexistence of Zn- and Cu-homometallic species in the same preparation. In our case, combined indirect evidence supports the feasibility of the second hypothesis for both the in vivo (Table 2) and the in vitro samples. First, it is difficult

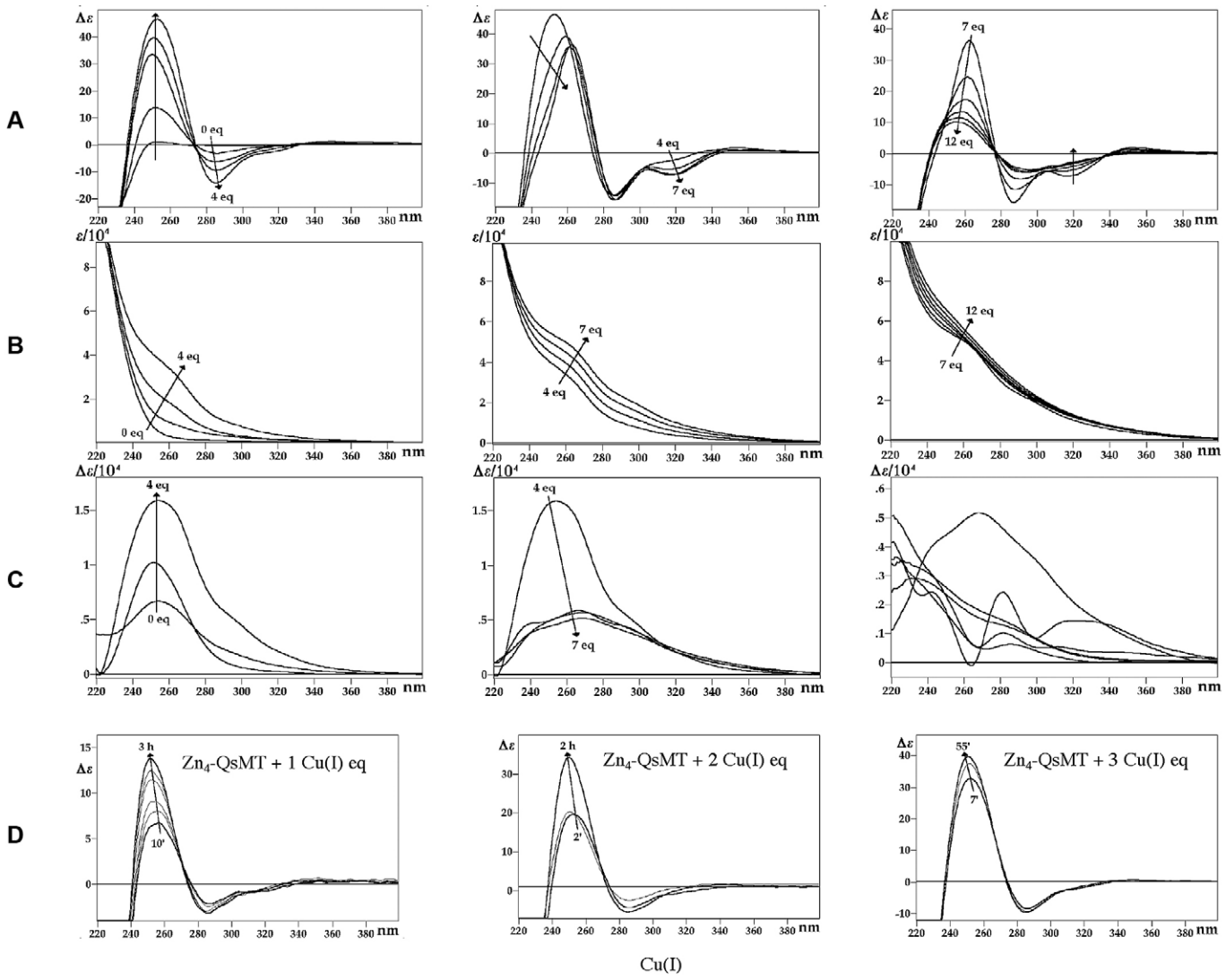

Fig. 3. (A) Circular dichroism, (B) UV–vis absorption, and (C) difference UV–vis absorption spectra recorded during the titration of Zn_4-QsMT with Cu(I) at pH 7. The arrows show the evolution of the spectra when the indicated number of Cu(I) equivalents was added. Spectra of (C) are obtained by subtracting the successive spectra of (B). (D) Evolution over time of the circular dichroism spectra corresponding to the addition of the first, second and third Cu(I) eq to Zn_4-QsMT at pH 7.

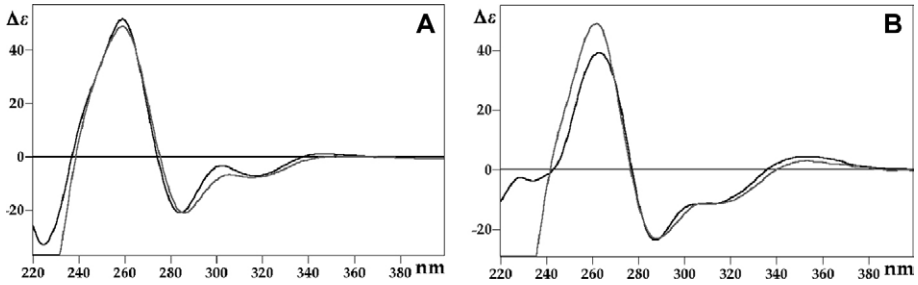

Fig. 4. Comparison of the CD spectra of several metal-QsMT complexes. (A) CD spectra of the recombinant Zn,Cu-QsMT (black solid line) and that obtained after the addition of five Cu(I) equivalents to Zn_4-QsMT (gray solid line). (B) CD spectra of the recombinant Cu–N25 (black solid line) and that obtained after the addition of seven Cu(I) equivalents to Zn_4-QsMT (gray solid line).

to explain why N25–C18 and QsMT should not fold into homometallic Cu(I) complexes considering that both independent N25 and C18 render homometallic Cu(I) species. Second, the lack of cooperativeness, as explained above, in the in vitro binding of the first four Cu(I) eq added to Zn_4-QsMT makes more likely that the M_4-species corresponds to a Zn_4-QsMT complex, and this is also in full agreement with the clear stoichiometric gap occurring between the M_4- and M_7-, M_8-, and M_9-species. Finally, it is remarkable that all CD spectra for homometallic Cu-species are very similar (Figs. 2C and 4B), closely resembling that of the MT4 mammalian Cu-thionein [26] but differing from those of heterometallic Zn,Cu-thio-

neins [44]. Therefore, and according to all these evidences, it seems logical to assume that M_7-, M_8- and M_9-correspond to homometallic Cu_7-, Cu_8- and Cu_9-species, and M_4- to a Zn_4-species. Consequently, we propose that the reaction for the Zn/Cu in vitro displacement in Zn_4-QsMT would follow the pathway: Zn_4-QsMT → Cu_7-QsMT → Cu_8-QsMT → Cu_9-QsMT.

Interestingly, it is worth noting that the displacement rate observed during the first steps of the Cu titration of Zn_4-QsMT (Fig. 3D) was very slow in comparison with similar reactions observed in animal MTs [21–23,26]. Specifically, instead of the conventional 10–20 min required to achieve thermodynamically stable species for each step of the Cu titrations of the corresponding Zn-MT aggregates, Zn_4-QsMT needed 3, 2 and 1 h to stabilize the first, second and third Cu(I) equivalents added, respectively (Fig. 3D). As a result, the *hairpin* fold proposed above for Zn-QsMT, including a stabilizing interaction of the spacer peptide, is now reinforced by the significant time-delay observed during the first steps of the Cu(I) titration of Zn_4-QsMT. This time dependency clearly differs from that caused by Hg(II) lability when this ion binds to mammalian MT1 [45]. The proposed interaction of the spacer with the metal aggregate would account for the Zn(II) ions remaining inaccessible, maybe deeply buried by the protein envelope and thus difficult to be displaced by Cu(I), despite the well-known higher affinity of copper for the SCys ligands. Only when the binding of the first Cu(I) ions had triggered Zn_4-QsMT unfolding, the peptide backbone would reach a higher mobility and progressively allow for a more easy access of Cu(I) to the SCys sites. Finally, this would also account for the coexistence of initial Zn_4-QsMT with the Cu_7-, Cu_8- and Cu_9-QsMT aggregates in the samples.

Our results show that although both N25 and C18 yield mixtures of homometallic Cu species, the latter needs to dimerize to achieve Cu-binding. This significant finding poses an intriguing question about the minimal length, number of Cys and peptide features required to form a fully-autonomous metal-binding domain. Fungal Cu-thioneins are the shortest MTs known, with 25 amino acids, seven of which are Cys [46]. These MTs yield in vivo Cu_6-complexes, while in vitro reconstitution suggests a 2–3 M(II) binding capacity. Now, we show that C18 (a 18-residue long peptide with six Cys) requires dimerization to bind Cu(I). Consequently, it can be proposed that a 18-residues peptide is too short to permit a monomeric fold that could bind, via its six Cys, a significant number of copper ions, probably showing different coordination environments. This dimerization requirement has been the basis for the proposal of a hairpin model for the full length QsMT in which it can be considered that metal binding is achieved after formation of a heterodimer between both Cys-rich domains. Contrasting with Cu(I) that can show different coordination environments (diagonal, trigonal or tetrahedral), Zn(II) binding usually gives rise to tetrahedral geometries, requiring more SCys donors and thus imposing lower metal/protein stoichiometric ratios. Enough examples of common inorganic complexes with a 2:6 Zn/thiolate ratio are found in literature. This, together with the fact that binding a reduced number of Zn(II) ions supposes a small volume to be wrapped by the protein, explain why dimerization of C18 is not strictly necessary when binding Zn(II) but required to bind Cu(I). Consequently, seven Cys in a 25-amino acids peptide remains the threshold for Cys-rich peptides to fold into stable Cu-monomeric aggregates. If we consider fungal MTs as representatives of the primordial Cys-rich metal-binding peptides in evolution, they might have evolved according to basic strategies. On one hand, an increase in the number of amino acids may have entailed the addition of adjacent Cys residues to this minimal number, resulting in autonomously folding domains (animal MTs). On the other hand, a longer intermediate peptide joining to two small Cys-rich regions may have led to the plant MT model, which depends on intramolecular domain dimerization.

3.3. Ability to complement metal sensitivity in yeast

S. cerevisiae contains a MT family comprised of the multicopy *CUP1* locus and the single *CRS5* gene, but both proteins are known to function mainly in copper detoxification, with a CUP1 efficiency far more significant than that of CRS5. Concomitantly, there is no evidence supporting the contribution of any yeast MT to zinc tolerance, being metal efflux and uptake into vesicles the primary mechanisms used by yeast cells to cope with an excess of this metal [47]. However, and in order to test the role of a plant MT to confer metal tolerance to a MT deficient yeast strain, $cup1^{\Delta}$ cells were transformed to express N25, C18, N25–C18 or QsMT. As a positive control we used a strain harboring only one copy of *CUP1* ($cup1^{S}$). Growth of $cup1^{\Delta}$ is inhibited at 75 μM Cu and that of $cup1^{S}$ at 300 μM Cu. On the other hand, cultures with Zn concentrations higher than 5 mM start to exhibit lower growth rates. Therefore, metal tolerance was evaluated by the ability of transformed $cup1^{\Delta}$ cells to grow in the presence of 75 μM $CuSO_4$ or 7 mM $ZnSO_4$.

When spotted in plates supplemented with 75 μM $CuSO_4$, $cup1^{\Delta}$ cells expressing QsMT showed a growth capacity similar to $cup1^{S}$, thus demonstrating an in vivo Cu-handling ability for the plant MT in yeast cells (Fig. 5A). However, at this copper concentration $cup1^{\Delta}$ cells expressing the N25–C18 chimera decreased their growth capacity compared to those expressing QsMT, which differs from N25–C18 in the spacer region. These results were unexpected since analyses of the N25–C18 metal aggregates showed Cu-binding capacity similar to QsMT, and suggest that the spacer peptide may play a significant role in the copper scavenging function of QsMT inside the yeast cell. As this role cannot be attributed to the copper binding capacity, stabilization or targeting of Cu-aggregates, as well as the possibility of molecular interaction with a second partner in the yeast/eukaryotic cell may be foreseen. Moreover, in silico predictions identify three phosphorilation and one myristoylation sites in the QsMT spacer sequence, and these are post-translation modifications widely accepted as plant protein signals for membrane targeting. A role in stabilization or cell targeting of the spacer, although underestimated in literature [48], would be consistent with the extremely high conservation of this region among plant MTs. Besides,

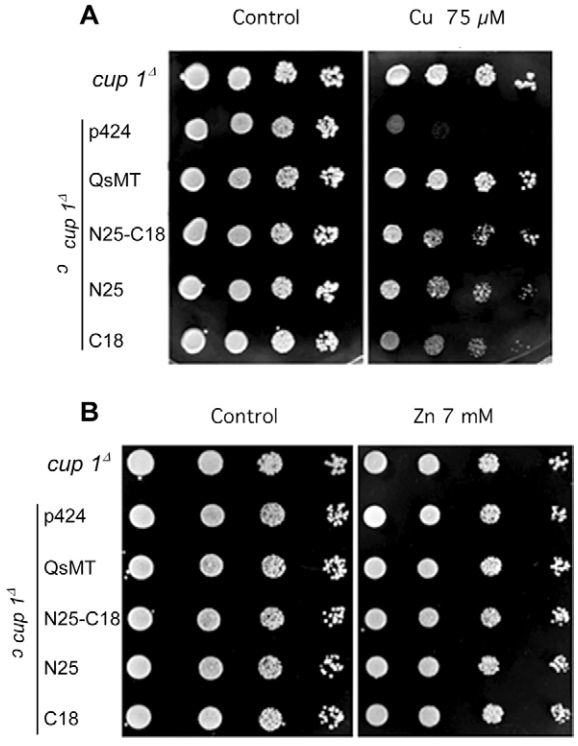

Fig. 5. Functional assays of metal tolerance complementation in yeast. Cultures of *cup1*^{S} and transformed *cup1*$^{\Delta}$ yeast cells with either the non-recombinant p424 vector or the same vector containing the sequences coding for QsMT, N25–C18, N25, and C18 were grown until an optical density at 600 nm of 0.5. Then, for each strain, 10-fold dilution series were spotted on SC agar plates containing (A) $CuSO_4$ 75 μM or (B) $ZnSO_4$ 7 mM. In each case, plates without added metal served as a control.

extensive in silico analyses have repeatedly failed to identify any non-plant MT protein with a region even partially similar to the plant MT spacer. The expression of the independent N25 and C18 peptides provided poorer Cu protection compared to QsMT and even to N25–C18, as otherwise expected for the lower number of cysteine residues. This is in accordance with the low chirality profile of the N25 CD spectra. The lowest detoxification capacity exhibited by C18 could also be related with the inability of the yeast cell to form or to adequately process intracellular dimeric aggregates.

It has been shown that MTs protect cells from oxidative stress by their capacity to scavenge reactive oxygen species (ROS), probably through the oxidation of cysteine thiols [49,50]. To test the protective capacity of QsMT against oxidative stress and the role of the protein domains, we subjected transformed yeast cells to paraquat and H_2O_2, since both oxidant treatments proved to highly induce *QsMT* gene expression in cork oak embryos [21]. Although these experiments were not conclusive, strains that expressed MTs (*cup1*$^{\Delta}$ cells expressing QsMT and *cup1*^{S} cells) tended to lower cell viability (data not shown). The addition of copper at non-toxic concentrations (5 μM $CuSO_4$) produced a slight protective effect in front of oxidative stress in all tested strains. These results are in agreement with previous observations [51] stating that, through their action as Cu-scavengers, MTs can impair the activation of Cu-dependent enzymes such as the copper–zinc superoxide dismutase (Cu–Zn SOD), a crucial agent for the antioxidant response.

Finally, the experiments to assess the possible protection role of QsMT or its derived peptides in front of deleterious Zn levels did reveal no significant differences between the untransformed and any of the transformed strains (Fig. 5B). This is in agreement with the null effect of the presence of the endogenous *CUP1* gene (Fig. 5B, first line), and also with the no participation of MTs in yeast zinc detoxification, a situation that, in this organisms, triggers other cellular pathways.

4. General conclusions

The results presented here are consistent with QsMT giving rise to homometallic Zn- and Cu-MT aggregates built according to a *hairpin* structure. The spacer region does not participate in metal coordination either in Zn_4-QsMT or in Cu_8-QsMT, although an insulating role in the former complex is suggested. On the other hand, Cu-sensitive yeast assays suggest that the spacer may play a role for Cu detoxification, possibly influencing QsMT stability or subcellular location. In conclusion, the overall results provide the first structure/function relationship characterization of physiological (Zn and Cu) metal binding features of a plant MT, including the first report of in vivo-conformed dimeric MT aggregates by ESI-MS, and of its capacity to complement copper sensitivity in yeast.

Acknowledgements

This work was supported by the *Spanish Ministerio de Ciencia y Tecnología* grants BIO2003-03892 for Silvia Atrian, AGL2003-00416 for Marisa Molinas and CTQ2004-00359/BQU for Mercè Capdevila. G.M. received a pre-doctorate fellowship from the *Pla de Formació de Personal Investigador del DURSI, Generalitat de Catalunya*. We are indebted to Laura Villarreal who kindly performed the titration of Zn_4-QsMT with Cu(I) and processed all the corresponding spectroscopical data. We also thank the *Serveis Científico-Tècnics de la Universitat de Barcelona* (ICP-OES, ESI-MS) and *Universitat de Girona* (DNA sequencing) for allocating instrument time.

References

[1] P.A. Binz, J.H.R. Kagi, http://www.biochem.unizh.ch/mtpage/MT.html (2001).
[2] N.J. Robinson, A.M. Tommey, C. Kuske, P.J. Jackson, Plant metallothioneins, Biochem. J. 295 (1993) 1–10.
[3] C. Cobbett, P.B. Goldsbrough, Phytochelatins and metallothioneins: roles in heavy metal detoxification and homeostasis, Annu. Rev. Plant Biol. 53 (2002) 159–182.
[4] J. Zhou, P.B. Goldsbrough, Structure, organization and expression of the metallothionein gene family in *Arabidopsis*, Mol. Gen. Genet. 248 (1995) 318–328.
[5] M. Chatthai, K.H. Kaukinen, T.J. Tranbarger, P.K. Gupta, S. Misra, The isolation of a novel metallothionein-related cDNA expressed in somatic and zygotic embryos of Douglas-fir: regulation by ABA, osmoticum, and metal ions, Plant Mol. Biol. 34 (1997) 243–254.

[6] C.A. Morris, B. Nicolaus, V. Sampson, J.L. Harwood, P. Kille, Identification and characterization of a recombinant metallothionein protein from a marine alga, *Fucus vesiculosus*, Biochem. J. 338 (1999) 553–560.
[7] P. Gonzalez-Duarte, Metallothioneins, in: J. McCleverty, T.J. Meyer (Eds.), Comprehensive Coordination Chemistry II, vol. 8, 2003, pp. 213–228.
[8] W.E. Rauser, Structure and function of metal chelators produced by plants: the case for organic acids, amino acids, phytin, and metallothioneins, Cell Biochem. Biophys. 31 (1999) 19–48.
[9] W.J. Guo, W. Bundithya, P.B. Goldsbrough, Characterization of the *Arabidopsis* metallothionein gene family: tissue-specific expression and induction during senescence and in response to copper, New Phytol. 159 (2003) 369–381.
[10] S.N.A. Abdullah, S.C. Cheah, D.J. Murphy, Isolation and characterisation of two divergent type 3 metallothioneins from oil palm, *Elaeis guineensis*, Plant Physiol. Biochem. 40 (2002) 255–263.
[11] C.N. White, C.J. Rivin, Characterization and expression of a cDNA encoding a seed-specific metallothionein in maize, Plant Physiol. 108 (1995) 831–832.
[12] M. Garcia-Hernandez, A. Murphy, L. Taiz, Metallothioneins 1 and 2 have distinct but overlapping expression patterns in *Arabidopsis*, Plant Physiol. 118 (1998) 387–397.
[13] J.M. Brkljacic, J.T. Samardzic, G.S. Timotijevic, V.R. Maksimovic, Expression analysis of buckwheat (*Fagopyrum esculentum* Moench) metallothionein-like gene (MT3) under different stress and physiological conditions, J. Plant Physiol. 161 (2004) 741–746.
[14] A. Murphy, L. Taiz, Comparison of metallothionein gene expression and nonprotein thiols in ten Arabidopsis ecotypes. Correlation with copper tolerance, Plant Physiol. 109 (1995) 945–954.
[15] N.A. van Hoof, V.H. Hassinen, H.W. Hakvoort, K.F. Ballintijn, H. Schat, J.A. Verkleij, W.H. Ernst, S.O. Karenlampi, A.I. Tervahauta, Enhanced copper tolerance in *Silene vulgaris* (Moench) Garcke populations from copper mines is associated with increased transcript levels of a 2b-type metallothionein gen, Plant Physiol. 126 (2001) 1519–1526.
[16] J. Zhou, P.B. Goldsbrough, Functional homologs of fungal metallothionein genes from *Arabidopsis*, Plant Cell 6 (1994) 875–884.
[17] R.C. Foley, Z.M. Liang, K.B. Singh, Analysis of type 1 metallothionein cDNAs in *Vicia faba*, Plant Mol. Biol. 33 (1997) 583–591.
[18] M. Ma, P.S. Lau, Y.T. Jia, W.K. Tsang, S.K.S. Lam, N.F.Y. Tam, Y.S. Wong, The isolation and characterization of Type 1 metallothionein (MT) cDNA from a heavy-metal-tolerant plant, *Festuca rubra* cv, Merlin, Plant Sci. 164 (2003) 51–60.
[19] J. Lee, D. Shim, W.Y. Song, I. Hwang, Y. Lee, *Arabidopsis* metallothioneins 2a and 3 enhance resistance to cadmium when expressed in *Vicia faba* guard cells, Plant Mol. Biol. 54 (2004) 805–815.
[20] P. Kille, D.R. Winge, J.L. Harwood, J. Kay, A plant metallothionein produced in *E. coli*, FEBS Lett. 295 (1991) 171–173.
[21] G. Mir, J. Domenech, G. Huguet, W.J. Guo, P.B. Goldsbrough, S. Atrian, M. Molinas, A Plant Type 2 metallothionein (MT) from cork tissue responds to oxidative stress, J. Exp. Bot. 55 (2004) 2483–2493.
[22] M. Valls, R. Bofill, N. Romero-Isart, R. Gonzalez-Duarte, J. Abian, M. Carrascal, P. Gonzalez-Duarte, M. Capdevila, S. Atrian, *Drosophila* MTN: a metazoan copper–thionein related to fungal forms, FEBS Lett. 467 (2000) 189–194.
[23] J. Domenech, O. Palacios, L. Villarreal, P. Gonzalez-Duarte, M. Capdevila, S. Atrian, MTO: the second member of a *Drosophila* dual copper–thionein system, FEBS Lett. 533 (2003) 72–78.
[24] M. Valls, R. Bofill, R. Gonzalez-Duarte, P. Gonzalez-Duarte, M. Capdevila, S. Atrian, A new insight into metallothionein classification and evolution. The in vivo and in vitro metal binding features of *Homarus americanus* recombinant MT, J. Biol. Chem. 276 (2001) 32835–32843.
[25] N. Cols, N. Romero-Isart, M. Capdevila, B. Oliva, P. Gonzalez-Duarte, R. Gonzalez-Duarte, S. Atrian, Binding of excess cadmium(II) to Cd7-metallothionein from recombinant mouse Zn_7-metallothionein 1. UV–VIS absorption and circular dichroism studies and theoretical location approach by surface accessibility analysis, J. Inorg. Biochem. 68 (1997) 157–166.
[26] L. Tio, L. Villarreal, S. Atrian, M. Capdevila, Functional differentiation in the mammalian metallothionein gene family, J. Biol. Chem. 279 (2004) 24403–24413.
[27] M. Capdevila, N. Cols, N. Romero-Isart, R. Gonzalez-Duarte, S. Atrian, P. Gonzalez-Duarte, Recombinant synthesis of mouse Zn_3-β and Zn_4-α metallothionein 1 domain and characterization of their cadmium (II) binding capacity, Cel. Mol. Life Sci. 53 (1997) 681–688.
[28] N. Romero-Isart, N. Cols, M. Termansen, J.L. Gelpi, R. Gonzalez-Duarte, S. Atrian, M. Capdevila, P. González-Duarte, Replacement of terminal cysteine with histidine in the metallothionein α and ß domain maintains its binding capacity, Eur. J. Biochem. 259 (1999) 519–527.
[29] S. Labbe, D.J. Thiele, Pipes and wiring: the regulation of copper uptake and distribution in yeast, Trends Microbiol. 7 (1999) 500–505.
[30] J. Bongers, C.D. Walters, D.E. Richardson, J.U. Bell, Micromolar protein concentrations and metalloprotein stoichiometries obtained by inductively coupled plasma. Atomic emission spectrometric determination of sulfur, Anal. Chem. 60 (1988) 2683–2686.
[31] R. Bofill, O. Palacios, M. Capdevila, N. Cols, R. Gonzalez-Duarte, S. Atrian, P. Gonzalez-Duarte, Zn(II) is required for the in vivo and in vitro folding of mouse Cu-metallothionein in two domains, J. Inorg. Biochem. 73 (1999) 57–64.
[32] D. Fabris, J. Zaia, Y. Hathout, C. Fenselau, Retention of thiol protons in two classes of protein zinc coordination centers, J. Am. Chem. Soc. 118 (1996) 12242–12243.
[33] V.D. Longo, E.B. Gralla, J.S. Valentine, Superoxide dismutase activity is essential for stationary phase survival in *Sacchraromyces cerevisiae*, J. Biol. Chem. 271 (1996) 12275–12280.
[34] D. Mumberg, R. Müller, M. Funk, Yeast vectors for the controlled expression of heterologous proteins in different genetic backgrounds, Gene 156 (1995) 119–122.
[35] T. Stearns, H. Ma, D. Botstein, Manipulating yeast genome using plasmid vectors, Methods Enzymol. 185 (1991) 280–297.
[36] C. Afonso, Y. Hathout, C. Fenselau, Evidence for zinc ion sharing in metallothionein dimers provided by collision-induced dissociation, Int. J. Mass Spectr. 231 (2004) 207–211.
[37] M. Capdevila, J. Domenech, A. Pagani, L. Tio, L. Villarreal, S. Atrian, Zn and Cd metallothionein recombinant species of the most diverse phyla may contain sulfide ligands, Angew. Chem. Int. Ed. Engl. 44 (2005) 4618–4622.
[38] L. Villarreal, L. Tio, S. Atrian, M. Capdevila, Influence of chloride ligands on the structure of Zn- and Cd-metallothionein species, Arch. Biochem. Biophys. 435 (2005) 331–335.
[39] C. Zhu, T. Lü, R. Zhang, N. Zhao, J. Liu, Modeling of kiwi fruit metallothionein kiwi503, Chin. Sci. Bull. 45 (2000) 1413–1417.
[40] K.B. Nielson, D.R. Winge, Independence of the domains of metallothionein in metal binding, J. Biol. Chem. 260 (1985) 8698–8701.
[41] C. Gruber, S. Stürzenbaum, P. Gehrig, R. Sack, P. Hunziker, B. Berger, R. Dallinger, Isolation and characterization of a self-sufficient one-domain protein (Cd)-metallothionein from *Eisenia foetida*, Eur. J. Biochem. 267 (2000) 573–582.
[42] B. Roschitzki, M. Vasak, A distinct Cu_4-thiolate cluster of human metallothionein-3 is located in the N-terminal domain, J. Biol. Inorg. Chem. 7 (2002) 611–616.
[43] A. Presta, A.R. Green, A. Zelazowski, M.J. Stillman, Copper binding to rabbit liver metallothionein. Formation of a continuum of copper(I)-thiolate stoichiometric species, Eur, J. Biochem. (Tokyo) 227 (1995) 226–240.
[44] R. Bofill, M. Capdevila, N. Cols, S. Atrian, P. Gonzalez-Duarte, Zn(II) is required for the in vivo and in vitro folding of mouse Cu-metallothionein in two domains, J. Biol. Inorg. Chem. 6 (2001) 405–417.
[45] A. Leiva-Presa, M. Capdevila, P. Gonzalez-Duarte, The mercury(II) binding to metallothioneins: variables governing the formation and structural features of the mammalian Hg-MT species, Eur. J. Biochem. 271 (2004) 4872–4880.
[46] K. Lerch, Copper metallothionein, a copper-binding protein from *Neurospora crassa*, Nature 284 (1980) 368–370.
[47] L.T. Jensen, W.R. Howard, J.J. Strain, D.R. Winge, V.C. Culotta, Enhanced effectiveness of copper ion buffering by CUP1 metallothionein

compared to CRS5 metallothionein in *Saccharomyces cerevisiae*, J. Biol. Chem. 271 (1996) 18514–18519.
[48] J.R. de Miranda, M.A. Thomas, D.A. Thurman, A.B. Tomsett, Metallothionein genes from the flowering plant *Mimulus guttatus*, FEBS Lett. 260 (1990) 277–280.
[49] L.S. Chubatsu, R. Meneghin, Metallothionein protects DNA from oxidative damage, Biochem. J. 291 (1993) 193–198.
[50] S. Hussain, W. Slikker, S.F. Ali, Role of metallothionein and other antioxidants in scavenging superoxide radicals and their possible role in neuroprotection, Neurochem. Int. 29 (1996) 145–152.
[51] T.D. Rae, P.J. Schmidt, R.A. Pufahl, V.C. Culotta, T.V. O'Halloran, Undetectable intracellular free copper: the requirement of a copper chaperone for superoxide dismutase, Science 284 (1999) 805–807.